Int. J. Electrochem. Sci., 14 **(2019)** 1591 – 1600, doi: 10.20964/2019.02.74

International Journal of
ELECTROCHEMICAL
SCIENCE
www.electrochemsci.org

Short Communication

Electrochemical Corrosion Behaviors of TiC Particles Reinforced Fe-based Composite Plasma Cladding Layers

Mingqi Tang[1,*], *Wen Wang*[2], *Gang Li*[1], *Zaiqiang Feng*[1], *Zhenwei Yan*[3], *Na Zhang*[1], *Ruizhu Zhang*[1]

[1] School of Materials Science and Engineering, North China University of Water Resources and Electric Power, Zhengzhou 450045, China
[2] School of Civil Engineering and Communication, North China University of Water Resources and Electric Power, Zhengzhou 450045, China
[3] School of Mechanical, North China University of Water Resources and Electric Power, Zhengzhou 450045, China
[*]E-mail: tangmq400@163.com

Received: 3 November 2018 / *Accepted:* 11 December 2018 / *Published:* 5 January 2019

In-situ and ex-situ titanium carbide (TiC) reinforced Fe-based cladding layers were fabricated via the plasma cladding method using nitrogen as the protective and reactant gas. In-situ TiC particles in the cladding layer were prepared using Ti and boron carbide (B_4C) powders as primary raw materials. The compositions, microstructures, and corrosion resistance of the cladding layers were compared. Results showed that in-situ TiC reinforced cladding layers consisted of α-Fe, Cr, Fe_3C, $Fe_{23}B_6$, $Fe_{23}(C,B)_6$, TiC and Ti(CN), whereas the cladding layers with ex-situ TiC consisted of α-Fe, Cr, $Cr_{23}C_6$, TiC, and Ti(CN). TiC and Ti(CN) particles were uniformly distributed in the two types of cladding layers. TiC, Ti(CN), and other ceramic phases reduced the relative area of α-Fe in the anode region of the cladding layer; hence, the surface rust layer was not easily peeled off, and the corrosion rate was effectively reduced. The corrosion resistance of the cladding layers significantly increased due to the formation of TiC particles and other compound phases. The Fe-based plasma cladding layer with in-situ TiC particles exhibited the best corrosion resistance.

Keywords: Plasma cladding, Composite layer, Titanium carbide, Corrosion behaviors

1. INTRODUCTION

The plasma cladding technique utilizes a high-temperature plasma arc to simultaneously melt the alloy powder and matrix surface metal. As the plasma arc is transferred, the molten metal rapidly solidifies to form a cladding layer that is metallurgically bonded to the matrix. The plasma cladding

technology can impart special physical, chemical, and mechanical properties to the surface of metal materials, thereby improving the service life of the resulting components and allowing the remanufacture of used and waste parts [1–3].

The ceramic particle-enhanced cladding layer utilizes the high strength, high hardness, and good toughness of the ceramic phase and exhibits excellent performance [4, 5]. The methods of synthesizing ceramic particles in the cladding layer are external addition (ex-situ) and in-situ synthesis. External addition refers to the addition of ceramic particles to the cladding alloy powder or molten pool, whereas in situ synthesis involves the synthesis of a ceramic-enhanced phase in the cladding layer via a chemical metallurgical reaction among various elements or compounds in the cladding material with a high-temperature plasma arc [6]. Studies have shown that various types of ceramic phase-reinforced cladding layers with different contents, morphologies, and distributions (e.g., WC, SiO_2, Al_2O_3, ZrO_2, TiC, TiV, TiN, Ti(C, N), and ZrB) can be obtained by tailoring the deposition materials, protective atmospheres, and cladding process parameters.

Among the enhanced phases, TiC and TiN have received extensive research attention. TiC can be wetted with molten Fe at high temperatures and presents several advantages, such as low formation free energy and easy synthesis. Its matrix structure occurs mostly in the form of dispersed particles [7–13]. TiN has high hardness, good corrosion resistance, dry lubrication resistance, and good biocompatibility. TiN is widely used as a protective film layer and enhanced phase in composite materials [14–17]. As a solid solution of TiC and TiN formed by the substitution of a C atom in TiC by N, Ti(CN) presents the combined advantages of TiN and TiC, including good toughness, excellent oxidation resistance, wear resistance, chemical stability, and self-lubricating property [18–21].

Wang et al. [7] used plasma cladding technology on the surface of Q235 steel to prepare an Fe-based alloy cladding layer with TiC enhanced phase. Here, the enhanced-phase TiC was mainly distributed in the grain and grain boundary, and the microhardness of the composite cladding layer reached 692 $HV_{0.2}$, which was considerably higher than that of the matrix (178 $HV_{0.2}$). Yin et al. [8] used the mixture of high chromium iron-based and Ti powder to fabricate laser cladding layers on 3Cr13. Their results showed that in-situ TiC can refine M_7C_3 grain size, increase bonding strength between the cladding layer and matrix, and improve the corrosion resistance and microhardness of the cladding layer. Vahdati Khaki et al. [9] prepared in-situ TiC-Al_2O_3 particles reinforced Fe-based composite cladding layers using the mixture of TiO_2, Al, C, and Fe powders as precursors via the gas tungsten arc welding method. Jiang et al. [10] used laser cladding and plasma cladding technologies to prepare TiC-enhanced composite cladding layers with the mixed powder of H13 tool steel and TiC as the cladding material on AISI4140 steel. The corrosion resistance of the cladding layer was greatly improved with increasing TiC content. Cao et al. [11] employed TiC as the enhanced phase in the cladding of nickel-based coatings, which also contain $M_{23}C_6$, chrome boride, and other hard phases. The maximum hardness of the cladding layer was 800 HV, which was five times that of the matrix material. Zhao et al. [12] utilized laser plasma cladding method to obtain an Fe-based cladding layer enhanced by TiC-VC composite particles on the surface of low carbon steel through the reactions between ferrotitanium, ferrovanadium, and graphite powders. Their results demonstrated a significant improvement in the wear resistance of the cladding layer. He et al. [17–19] used N_2 as the protective and reactive gas during plasma spraying and Ti and graphite powders as raw materials to prepare in-situ synthesized Ti(CN)-reinforced composite layers via

the reactive plasma spraying method; such layers exhibited high hardness, high toughness, and excellent wear resistance.

Previous studies primarily focused on the mechanical properties, especially the tribological behavior and wear resistance, but only few investigated the influence of addition methods (in-situ or ex-situ), morphologies, and distributions of TiC particles on the corrosion resistance of composite cladding layers. In this study, TiC powder, and the mixture of Ti and boron carbide (B_4C) powder were used as additives for an Fe-based alloy powder to prepare ex-situ and in-situ TiC reinforced composite cladding layer via plasma cladding method, respectively. N_2 was used during plasma cladding as the reactant and protective gas. The microstructures, compositions and corrosion behavior of the cladding layers were investigated.

2. EXPERIMENTAL PROCEDURES

Q235 steel plates with size of 200 mm × 100 mm ×10 mm were used as substrate materials. The plates were ground before plasma cladding using SiC abrasive paper (300 meshes) for rust removal and then ultrasonically cleaned in acetone. Fe-based alloy powder (Fe310, Beijing Research Institute of Mining) with a particle size of −140 to +320 mesh was used as the basic material, and its chemical compositions are listed in Table 1. The mixture of Ti (99.9% in purity), B_4C (99.9% in purity), and Fe310 (90 wt.% mass fractions) powders was used to prepare for the in-situ synthesis of TiC reinforced plasma cladding layer. The mass ratio of Ti and B_4C powders was 1:2.6. The mixture of Fe310 (90 wt.% mass fractions) and TiC powders (99.9% in purity) was used to prepare for the ex-situ TiC reinforced cladding layer. The particle size of TiC, Ti, and B_4C powder was about 2–3 μm.

Table 1. Chemical composition of Fe310(wt%)

Cr	C	B	Si	Fe
15	0.1	1	1	balance

The configured alloy powder was thoroughly mixed with water glass ($Na_2O{\cdot}nSiO_2$) blinder and preset to the 2–3 mm substrate surface. The prepared preset layer was dried naturally for 24 h and baked at 100°C for 1 h and at 150°C for 1 h. The plasma cladding layers were prepared using plasma cladding equipment (IGS600, Igood China). The parameters of plasma cladding were as follows: voltage, 80 V; current, 250 A; and protective gas nitrogen flow, 6 $L{\cdot}min^{-1}$.

X-ray diffraction (XRD, Bruker D8 ADVANCE) with Cu Kα radiation was conducted to study the phase constitution of the plasma cladding layers. Continuous scanning with a 4° min^{-1} scanning speed in the 2θ range between 30° and 90° was adopted. The morphologies and compositions of the cladding layers were investigated by scanning electron microscopy (FEI Quanta 2000) with energy dispersive spectroscopy (EDS OXFORD LINK ISIS).

The corrosion behavior of the cladding layers in 3.5 wt.% NaCl solution was tested by using a CHI-660E electrochemical workstation in a three-electrode system electrolytic cell at room temperature

(25 °C). The cladding layer had a 1 cm^2 exposed area, and its remaining parts were sealed using silicone rubber. The auxiliary electrode and the reference electrode were platinum foil and saturated calomel, respectively. Potentiodynamic polarization tests were carried out from cathodic to anodic at the speed of 1 $mV \cdot s^{-1}$. Electrochemical impedance spectroscopy (EIS) measurements were conducted at 100 kHz – 0.01 Hz with the applied 10 mV signal amplitude at open circuit potential after the cladding layers were immersed in NaCl solution for different times.

3. RESULTS AND DISCUSSION

Fig. 1 shows the XRD patterns of the different cladding layers. The base cladding layer was mainly composed of α-Fe and Cr. The cladding layer with in-situ TiC was mainly composed of α-Fe, Cr, Fe_3C, $Fe_{23}B_6$, $Fe_{23}(C,B)_6$, TiC, and Ti(CN) phases. The main constituent phases of the cladding layer with ex-situ TiC were α-Fe, Cr, Fe_3C, $Cr_{23}C_6$, TiC, and Ti (CN), and the Ti(CN) phase contained therein was mainly composed of $Ti(C_{0.3}N_{0.7})$ and $Ti(C_{0.2}N_{0.8})$. Diffraction peaks associated with Ti and B_4C were not found in the XRD patterns, which indicated that these phases were fully involved in the metallurgical reaction in the high temperature molten pool.

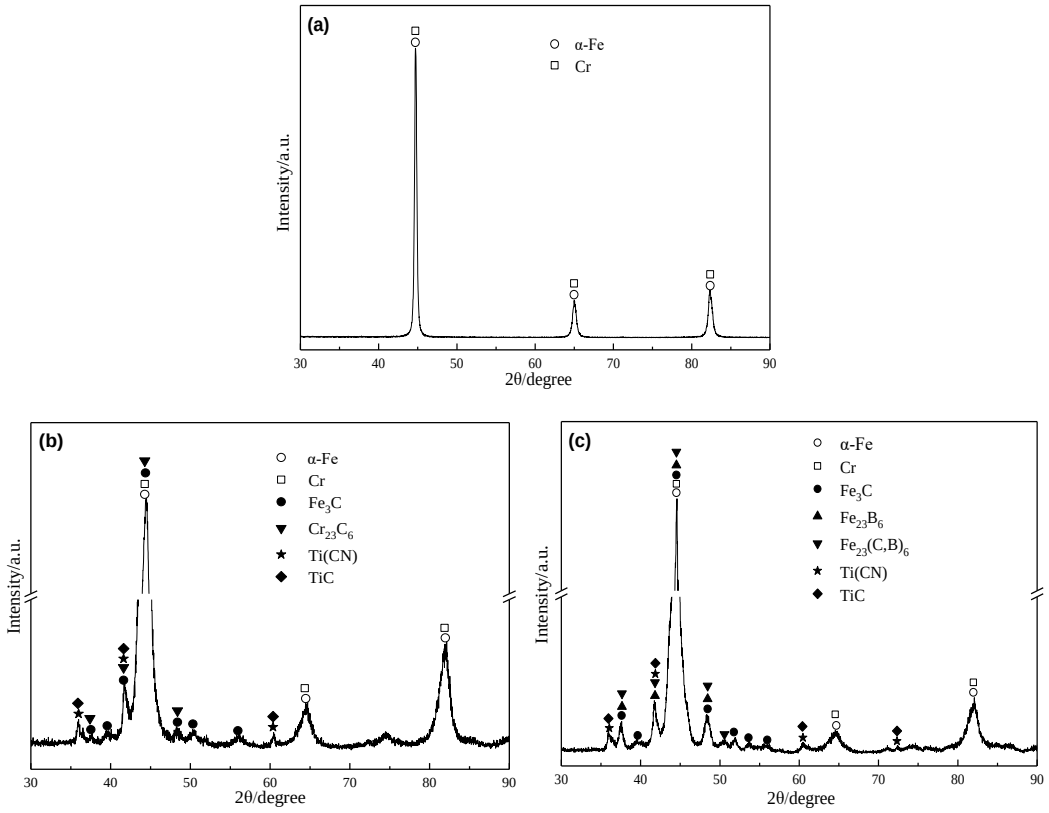

Figure 1. XRD patters of the cladding layer, (a) base layer, (b) with ex-situTiC and (c) with in-situ TiC.

The cladding material and surface layer of substrate were melted during the plasma cladding under the high temperature of the plasma arc to form a molten pool. A series of complex physical and

chemical reactions between the original compounds occurred to form new compounds. Compared with the base cladding layer, besides the diffraction peak of TiC in the cladding layer containing TiC powder, the diffraction peaks of Fe_3C, $Cr_{23}C_6$, and Ti(CN) also appeared. This finding may be attributed to a portion of TiC that decomposed into Ti and C under the high temperature of the plasma arc during the cladding process and C that reacted with Fe and Cr in the Fe-based powder to form Fe_3C and $Cr_{22}C_6$ [22]. TiC in the high-temperature molten pool was also partially dissolved such that the alloy melt was supersaturated with Ti and C. Similarly, B_4C in the cladding material decomposed into B and C under high temperature. C reacted with Ti to form TiC, and B reacted with Fe and C in the molten pool to form $Fe_{23}B_6$ and $Fe_{23}(C,B)_6$. N_2 was the protective gas used during plasma cladding, and it reacted with Ti to form TiN at high temperature. The in-situ synthesis of Ti(CN) in the cladding layer could be described by the following chemical reactions:

$$Ti + C = TiC \quad (1)$$

$$2Ti + N_2 = 2TiN \quad (2)$$

$$xTiC + (1- x)TiN = TiC_xN_{1-x} \quad (3)$$

Reactions (1) and (2) were carried out spontaneously in the high temperature molten pool. According to the relevant thermodynamic data, TiC is easily generated at temperatures above 2000 K, and TiN may be generated below 2000 K [23]. Some of the TiC and TiN in the molten pool may undergo a solid-solution reaction (3) to form Ti(CN) because they have the same crystal structures.

Fig 2(a) shows a clear white bright band at the bonding interface between the substrate and cladding layer, this band was attributed to the surface layer of the matrix that melted during the cladding process. When the plasma arc was swept over the reaction system, supercooling of the related region was the highest after the molten pool solidified. Similarly, the temperature gradient G in this region was the largest, the solidification velocity *R* was the smallest (approaching 0), and the shape factor G/R was the highest; these characteristics promoted the instantaneous formation and growth of a large number of crystal nuclei. The nuclei rapidly aggregated and could not continue to grow; thus, they formed a very thin equiaxed crystal region. As solidification and crystallization continued, the fine-grained zone absorbed and released heat. Upon removal of the heat source, the temperature gradient became more gradual, thereby decreasing *G* and increasing *R*; hence, *G*/*R* gradually decreased. At this time, columnar crystals and dendrites formed, as shown in Fig. 2(b). The cladding layer with ex-situ TiC consisted of α-Fe, Cr, acicular martensite structure, and numerous dispersed black particles. The particle size is approximately 10 μm. The cladding layer with in-situ TiC consisted of α-Fe, acicular martensite structure, continuous network or chrysanthemum-shaped boride, boron carbide, and a large amount of dispersed black particles with a particle size of approximately 10 μm. EDS analysis of the black particles in the above cladding layer revealed that the main components were Ti, C, and N. Meanwhile, the results of XRD analysis demonstrated that the black particles in the cladding layer were TiC and Ti(CN).

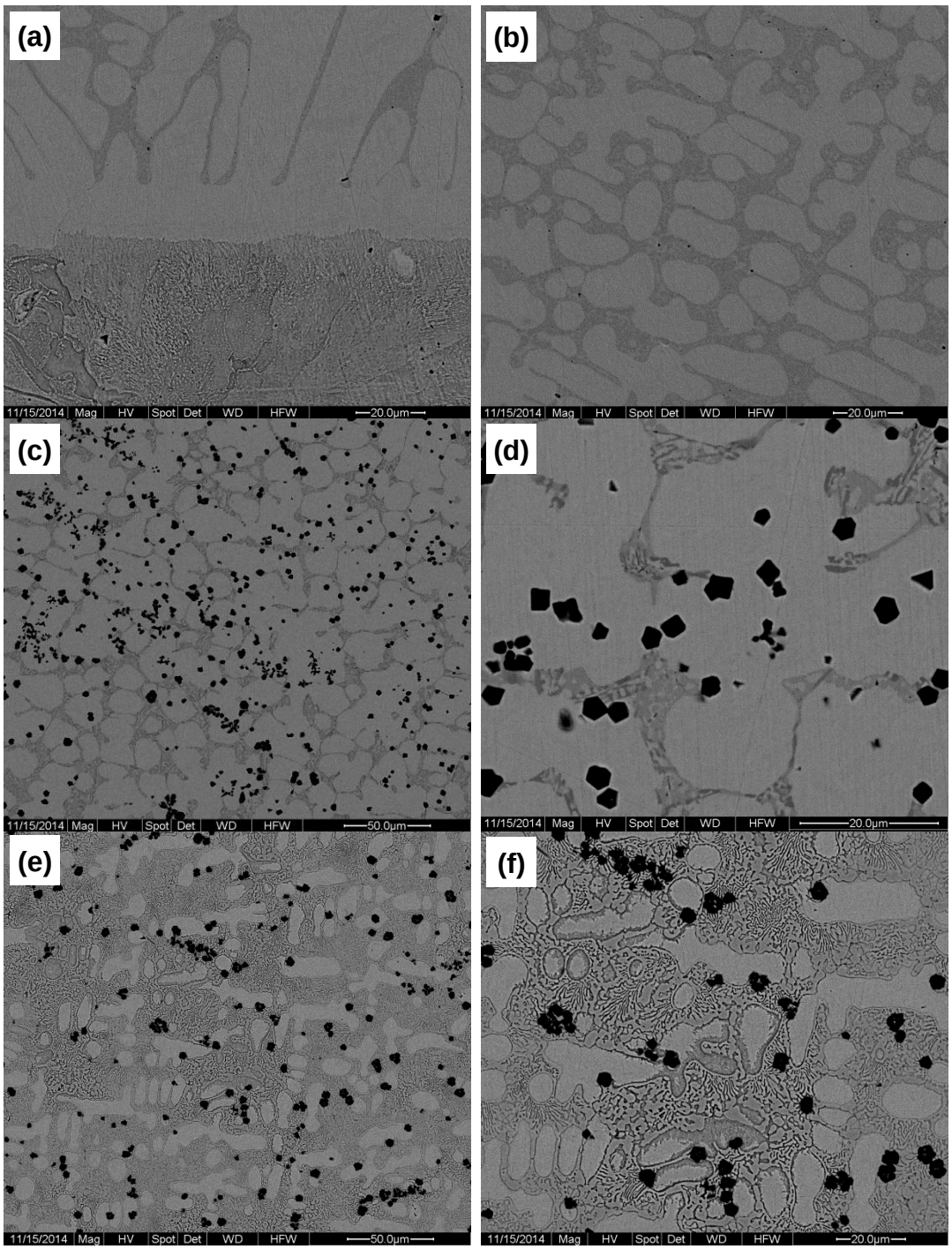

Figure 2. Microstructures of cladding layers, (a,b) base layer, (c,d) with ex-situ TiC and (e, f) with in-situ TiC.

Fig. 3 shows the Tafel polarization curve of different cladding layers in 3.5 wt.% NaCl solution. Table 2 shows the corrosion current densities and corrosion potentials of the cladding layers. The high corrosion potential and low corrosion current density of the cladding layer suggest good corrosion resistance. The corrosion potential of the cladding layer increased, and its corrosion current decreased with the addition of TiC and Ti+B_4C in the raw materials. Thus, the ex-situ and in-situ TiC cladding layers demonstrated better corrosion resistance in 3.5 wt.% NaCl solution than the base cladding layer.

Compared with α-Fe and Cr, TiC, Ti(CN), Fe_3C, $Cr_{23}C6$, $Fe_{23}B_6$, and $Fe_{23}(C,B)_6$ presented better chemical stability. The formation of such compounds could decrease the area occupied by α-Fe and Cr, thereby reducing the corrosion current of the resulting layer.

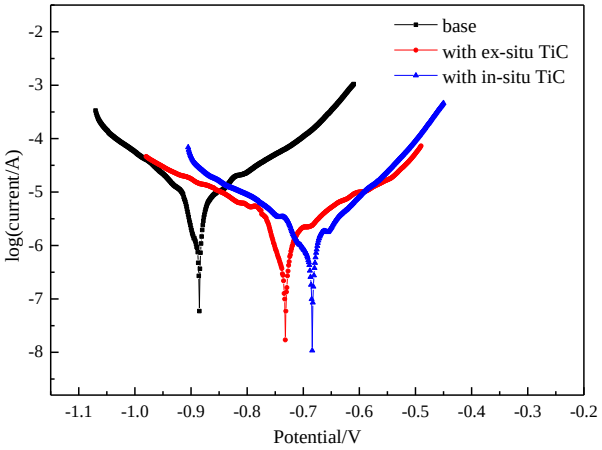

Figure 3. Polarization curves of the cladding layers in 3.5 wt% NaCl solution

Table 2. Analysis results of the potentiodynamic polarization curves

Sample	E_{corr} (V)	i_{corr} (mA/cm^2)
Substrate	-0.883	8.55×10^{-6}
With ex-situ TiC	-0.732	2.14×10^{-6}
With in-situ TiC	-0.688	1.11×10^{-6}

Fig. 4 shows the Nyquist spectra of the cladding layers in 3.5 wt.% NaCl solution with different immersion times. All cladding layers exhibited similar electrochemical corrosion behavior. With prolonged immersion time, the real inductance in the low-frequency region decreased, which indicated that corrosion occurred on the cladding layer surface. The corrosion products that were mainly composed of unstable γ-FeOOH formed a rust layer [24]. The rust layers became thicker with prolonged immersion time, and active γ-FeOOH was transformed into inactive α-FeOOH; a stratified dual rust-layer with a porous outer layer and dense inner layer also formed [25]. As shown in Fig. 4, the inductive contraction characteristics were converted into capacitive reactance characteristics. The thick rust layer formed on the cladding layer surface, which blocked the diffusion of Cl^- ions into the anode region and showed diffusion characteristics. The outer rust layer was desquamated because of its loose construction. Thus, trend of the capacitive loop diameter of the cladding layers showed an initial increase and subsequent decrease with prolonged immersion time.

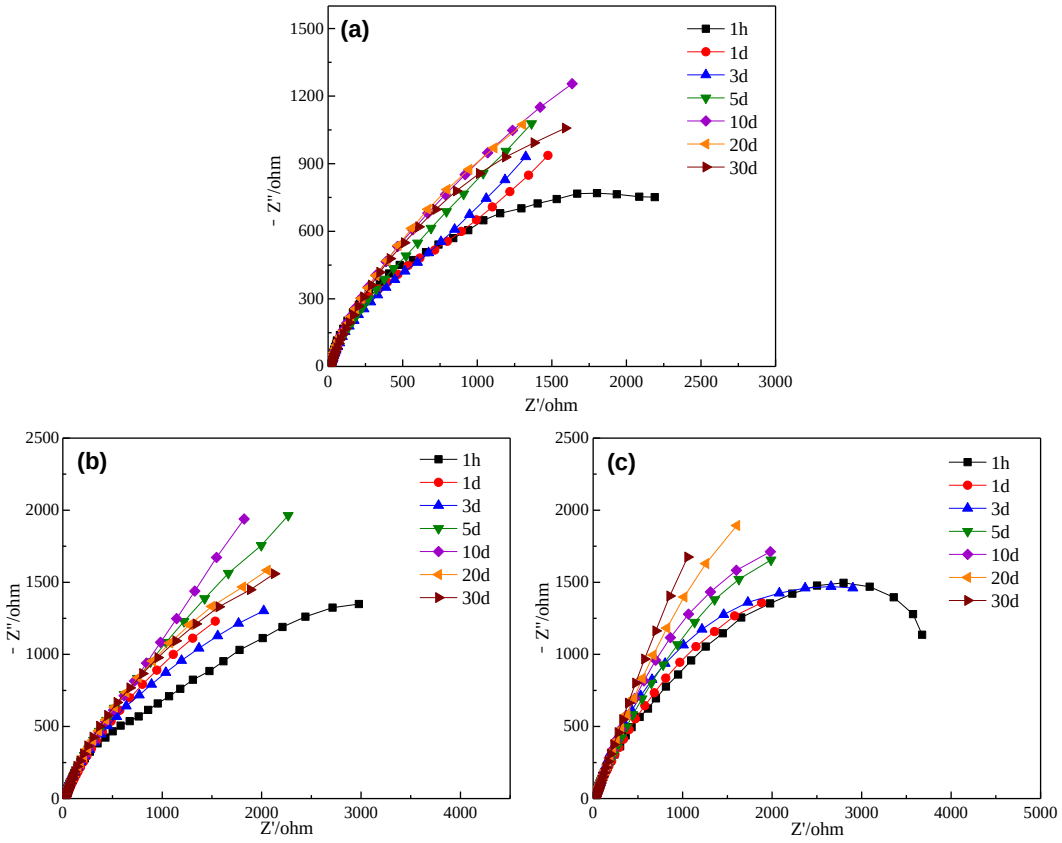

Figure 4. Nyquist spectra of the cladding layers immersed in 3.5 wt.% NaCl solution for different time, (a) base layer, (b) with ex-situ TiC and (c) with in-situ TiC.

The EIS data were fitted using an equivalent circuit as shown in Fig. 5. R_s represents the solution resistance, R_p is the resistance of the porous outer layer, CPE_1 is the total surface capacitance of the electrode considering the dispersion effect, CPE_2 is the "solution/metal" interface capacitance, and R_t is the reaction resistance or charge transfer resistance. The dense inner layer or passive film determines the values of R_t [26]. The polarization resistance of the rust layer is decided by the sum of R_p and R_t [27,28]. The variations in R_p and R_t with immersion time are shown in Fig. 6. In this experiment, R_p was about 6–550 $\Omega \cdot cm^2$, which was small compared with R_t. Thus, the R_t values could be used to reflect the variation in the corrosion resistance of the cladding layers during immersion. R_t of the cladding layers showed similar trends during the whole immersion process. Several fluctuations occurred in the later stages of immersion due to the alternating processes of new rust formation, protective rust layer formation, and partial shedding. R_t of the base cladding layer was lower than that of the cladding layers with ex-situ and in-situ TiC during this stage, and its surface was covered with a thick rust layer. At the same time, a passive film formed. However, the rust layer was loose and offered poor protection; new rust sites were continuously generated, resulting in the relatively uniform overall corrosion of the matrix and decreased R_p of the base cladding layer. This phenomenon may be attributed to the addition of TiC and Ti+B_4C to the cladding material, which caused the emergence of TiC, Ti(CN), Fe_3C, $Cr_{23}C_6$, $Fe_{23}B_6$, $Fe_{23}(C,B)_6$, and other compound phases in the cladding layer. The phase constituents directly influenced the formation of passive film on the surface of the cladding layer, and the stable and dense passive film suggested excellent corrosion resistance [29]. Compared with the potential of these compounds, that of

α-Fe is low, suggesting that this phase may form numerous corrosion micro-cells and corrode into Fe ions as a micro-anode. Studies have shown that increasing the TiC and TiN content in the cladding layer does not change the corrosion mechanism [30, 31]. However, increasing the content of TiC and Ti(CN) in the cladding layer reduced the relative area of the α-Fe anode region, thereby reducing the corrosion current and increasing the potential. A small anode area also minimized the likelihood that the rust layer would peel off, and the surface showed strong corrosion resistance. As a result, the cladding layer with in-situ TiC exhibited the highest corrosion resistance.

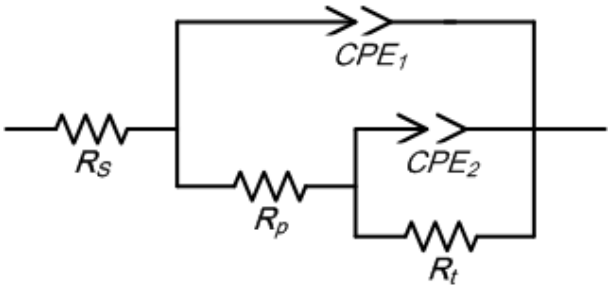

Figure 5. Equivalent circuit of the cladding layers being immersed in 3.5 wt% NaCl solution.

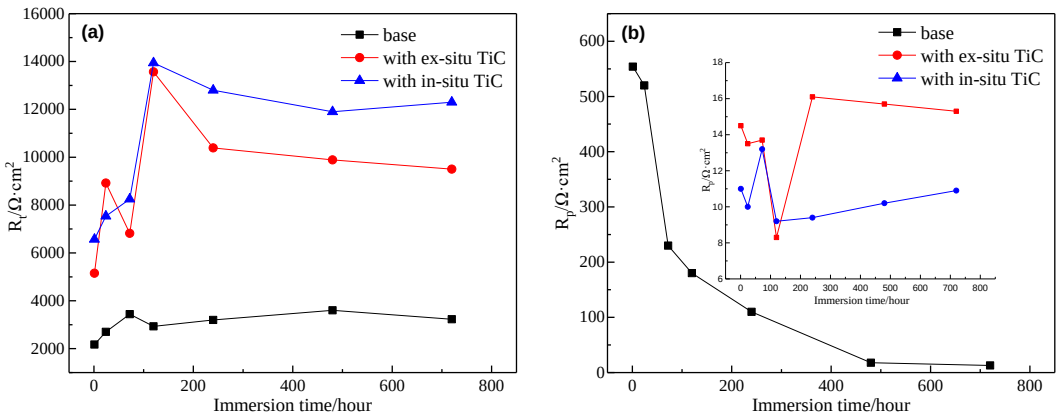

Figure 6. Reaction resistance R_t (a) and R_p (b) variation of three cladding layers with immersion time,

4. CONCLUSIONS

1. The cladding layer prepared from Fe-based alloy was mainly composed of α-Fe and Cr. The addition of TiC and Ti+B_4C led to the emergence of several phases, including TiC, Ti(CN), Fe_3C, $Cr_{23}C_6$, $Fe_{23}B_6$, and $Fe_{23}(C,B)_6$, in the cladding layer. In this study, TiC and Ti(CN) were dispersed.

2. The formation of ex-situ and in-situ TiC and other compounds increased the self-corrosion potential, reduced the corrosion current, and increased the corrosion resistance of the resulting cladding layer compared with those of the base cladding layer.

3. The corrosion resistance was effectively increased due to the formation of stable and dense passive film on the cladding layer with ex-situ and in-situ TiC.

ACKNOWLEDGMENT
This work was supported by the National Natural Science Foundation of China (Grant No. 51301070), Engineering Technology Research Center of Henan Province ([2016]221-35), Project for University Young Key Teacher of Henan Province (No. 2015GGJS-106) and Key Program of Henan Provincial Department of Education (18A430018).

References

1. C Zhao, F. Tian, H. Peng, J. Hou, *Surf. Eng. Coat. Tech.,* 155(2002)80–84.
2. G. Xu, M. Kutsuna, Z. Liu, H. Zhang, *Mat. Sci. Eng. A*, 417(2006)63–72.
3. D. Chen, D. Liu, Y. Liu, H. Wang, Z. Huang, *Surf. Eng. Coat. Tech.,* 239(2014)28–33.
4. J. Li, C. Chen, Z. Lin, S. Tiziano, *J. Alloys. Compd.*, 509(2011)4882–4886.
5. B. Du, Z. Zou, X. Wang, S. Qu, *Appl. Surf. Sci.,* 254 (2008) 6489–6494.
6. M.M. Savalani, C.C. Ng, Q.H. Li, H.C. Ma, *Appl. Surf. Sci.*, 258(2012)3173–3177.
7. A. Emamian, S.F. Corbin, A. Khajepour, *Surf. Eng. Coat. Tech.,* 206(2012)4495–4501.
8. Z.X. Wang, W.T. Yang, W. Fang, J. Lu, *Hot working tech*., 39(2010)50–52. (in chinese)
9. Y. Yin, C. Pan, R. Zhang, C. Zhao, Y. Qu, *J. Alloys. Compd.*, 765(2018)782–790.
10. M. Sharifitabar, J. Vahdati Khaki, M. Haddad Sabzevar, *Surf. Eng. Coat. Tech.,* 285(2016)47–56.
11. W. Jiang, R. Kovacevic, *J. Mater. Process. Tech.*, 186(2007)331–338.
12. K. Chong, H. Zhang, G. Xiao, H. Xu, W. Zhao, *Int. J. Electrochem. Sci.*, 13(2018) 6858–6869.
13. Y. Cai, Z. Luo, Y. Chen, S. Ao, *Surf. Eng.*, 33(2017)936–943.
14. J.A. Vreeling, V Ocelík, J.T.M. De Hosson, *Acta Mater.*, 50(2002)4913–4924.
15. D. Liu, M. Li, J. Huang, H. Chen, R. Sun, Z. Li, *Chinese J. Las.*, 44(2017)123–129. (in chinese)
16. W. Cui, Y. Zhang, R. Song, P. Wang, *Ceram. Int.,* 44 (2018) 14767–14773.
17. A. Hefnawy, N. Elkhoshkhany, A. Essam, *J. Alloys. Compd.*, 735 (2018) 600–606.
18. P. Huber, D. Manova, S. Mändl, B. Rauschenbach, *Surf. Coat. Tech.,* 174(2003)1243–1247.
19. P. Mi, J. He, Y. Qin, K. Chen, *Surf. Coat. Tech.,* 309(2017)1–5.
20. Y. Qin, G. Zheng, L. Zhu, J. He, F. Zhang, Y. Dong, F. Yin, *Surf. Coat. Tech.*, 342(2018)137–145.
21. F. Zhang, J. He, K. Chen, Y. Qin, C. Li, F. Yin, *Appl. Surf. Sci.*, 427(2018)905–914.
22. Y. Wu, *Trans. China Weld. Inst.*, 22(2001)89–92. (in chinese)
23. Y. Yang, W. Yao, J. Liu, H. Zhang, *J. Northeast Univ: Nat. Sci. Ed.*, 31(2010)1165-1169. (in chinese)
24. Y.H. Qian, D. Niu, J.J. Xu, M.S. Li, *Corros. Sci.,* 71(2013)72-77.
25. D. de la Fuente, J. Alcántara, B. Chico, I. Díaz, J.A. Jiménez, M. Morcillo, *Corros. Sci.,* 110 (2016) 253–264.
26. C. Man, C. Dong, T. Liu, D. Kong, D. Wang, X. Li, *Appl. Surf. Sci.*, 467–468(2019)193-205.
27. C. W. Du, X.G. Li, P. Liang, Z.Y. Liu, G.F. Jia, Y.F. Cheng, J.Mater. Eng. Perform., 18(2009)216-220.
28. H. Qian, D. Zhang, Y. Lou, Z. Li, D. Xu, C. Du, X. Li, *Corros. Sci.,* 145(2018)151–161.
29. S. Zhou, Y. Xu, B. Liao, Y. Sun, X. Dai, H. Pan, *J. Alloys. Compd.*, 768(2018)697-706.
30. G.N.K.Ramesh Bapu, S. Jayakrishnan, *Surf. Coat. Tech.*, 206(2012) 2330–2336.
31. W. Chen, J. Zhou, M. Hu, *Rare Metal Mat. Eng.*, 42(2013)2068–2072.